Available online at www.sciencedirect.com
ScienceDirect
Trans. Nonferrous Met. Soc. China 26(2016) 627−633
Transactions of Nonferrous Metals Society of China
www.tnmsc.cn

Effect of pre-annealing on microstructure evolution of TRC AA3003 aluminum alloy subjected to ECAP

Michaela Šlapáková POKOVÁ, Mariia ZIMINA, Miroslav CIESLAR

Faculty of Mathematics and Physics, Charles University in Prague, Ke Karlovu 5, 121 16 Prague 2, Czech Republic

Received 15 April 2015; accepted 14 October 2015

Abstract: An AA3003 aluminum alloy prepared by twin-roll casting was modified by a small amount of zirconium. Annealing at 450 ℃ led to precipitation of coherent Al_3Zr phase and a simultaneous co-precipitation of Mn-rich α-Al(Mn,Fe)Si phase. Severe plastic deformation by equal channel angular pressing resulted in the grain refinement and increase of microhardness. Observation by electron back-scatter diffraction and in-situ transmission electron microscopy revealed influence of pre-annealing on microstructure changes during post-deformation heat treatment. Dislocation recovery and precipitation of α-Al(Mn,Fe)Si particles preceded recrystallization at 450 ℃ in material which was not annealed before deformation. The pre-deformation annealing enabled dynamic recovery during deformation as it depleted the solid solution from Mn atoms. Recrystallization was enhanced by Al_3Zr precipitates.

Key words: aluminum alloy; Al_3Zr; α-Al(Mn, Fe)Si; pre-annealing; recovery; recrystallization; microstructure evolution

1 Introduction

The production of materials with fine grain size is of a great importance. The reduction of the grain size results generally in a strength increase at low temperatures and in a formability enhancement at elevated temperatures. The most common method for grain refinement of aluminum alloys is severe plastic deformation (SPD), which can produce grains smaller than 1 μm.

The most often used SPD technique is equal channel angular pressing (ECAP) [1−3]. It is a process during which a billet is pressed through a special die consisting of two channels of the same cross-section, which intersect at an angle of Φ ($90° \leq \Phi < 180°$). The shape of the billet remains nearly unchanged after the pressing [4]. The ECAP procedure can be thus repeated several times and the stored deformation energy can be multiplied. Consequently, ultra-fine grained material with a high fraction of high-angle grain boundaries can be produced. The strength of the material after ECAP is affected not only by the presence of the second phase particles, low-angle and high-angle grain boundaries and texture, but also by the solid solution saturation, which is given by the previous heat treatment [5].

The present study is focused on a new class of twin-roll cast (TRC) aluminum alloys from AA3003 series with manganese, iron and silicon as main alloying elements, modified by an addition of zirconium. TRC is less demanding on the amount of energy and material used during manufacturing than direct-chill casting (DC), therefore, there is a growing interest in the application of TRC materials. However, the initial microstructure of TRC strips differs significantly from that of the DC ones and has been intensively studied in recent years [6−10]. The high solidification rate around 500 K/s results in the microstructure refinement and formation of finely dispersed primary particles and high solid solution supersaturation [11].

For technical applications the high temperature stability of the deformed microstructure is required [12]. Recovery and recrystallization processes in Al-based alloys can be significantly suppressed by the addition of small amount of Zr and/or Sc. A dense dispersion of coherent Al_3Zr, Al_3Sc or $Al_3(Zr_xSc_{1-x})$ particles can retard both the movement of lattice dislocations and grain boundaries and thus contribute to a better stability of the microstructure at elevated temperatures [13,14]. Especially, the suppression of the grain growth is of great importance in materials where superplastic deformation should be achieved. Because of limited resources and

Corresponding author: Michaela Šlapáková POKOVÁ; E-mail: pokova@karlov.mff.cuni.cz
DOI: 10.1016/S1003-6326(16)64151-1

high price of Sc, usually, only Zr as an additional alloying element is used. Nevertheless, only scarce information is accessible for Zr-containing TRC Al materials [15,16]. Moreover, no results are at present available on the application of ECAP or other SPD techniques on TRC Al-based materials, although combinations of high supersaturation due to TRC and ultra-fine grained structure formed by SPD and stabilized by Al_3Zr dispersion may generate materials with superior properties.

2 Experimental

A standard AA3003 aluminum alloy with addition of 0.16% Zr (mass fraction) cast by the TRC method into a strip of about 10 mm in thickness was used in this work. This alloy will be referred as Material A. The as-cast structures consist of large subgrains with relatively high dislocation density in their interiors and almost no particles of secondary phases [17].

The alloy was annealed in an air furnace with a rate 0.5 K/min to 450 ℃, held at 450 ℃ for 8 h and subsequently water-quenched in order to induce the precipitation of Al_3Zr phase (Fig. 1) [18]. The annealed alloy will be referred as Material B. The annealing also led to the precipitation of numerous Mn and Si-rich particles of cubic α-Al(Mn,Fe)Si phase, which are generally observed in AA3003 alloys after the high temperature annealing [19,20].

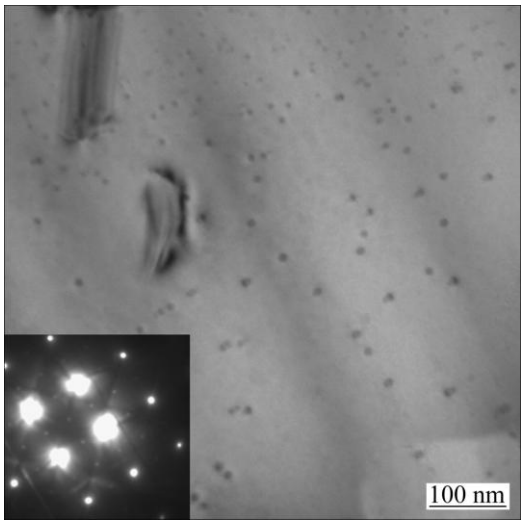

Fig. 1 Precipitates of Al_3Zr phase formed during pre-annealing at 450 ℃ (Inset represents selected area electron diffraction near $[100]_{Al}$ zone axis)

Both as-cast and annealed materials were subjected to severe plastic deformation by ECAP at room temperature. The used ECAP channels had a square cross-section of 10 mm × 10 mm and they intersect at an angle of 90°. A pressing speed of 10 mm/min and route B_C were applied, while the specimen was rotated after each pass by an angle of 90 °around its axis [4].

The main aim of this work is to evaluate the influence of pre-ECAP annealing on the microstructure and mechanical properties evolution of the alloy after ECAP. In order to investigate thermal stability of the alloy at elevated temperatures, the deformed materials were step-by-step isochronally annealed in an air furnace with a heating scheme of 50 K/50 min.

The measurement of Vickers microhardness ($HV_{0.1}$) with a load of 100 g at QNess 10A, electron back-scatter diffraction (EBSD) in scanning electron microscope FEI Quanta FEG 200 and in-situ heating in transmission electron microscope JEOL 2000FX (TEM) with the same heating scheme as the one employed during isochronal annealing were used for the material characterization. For the microhardness measurement, 10 indents on each sample were performed. The scanned area by EBSD was either 250 μm × 250 μm with a step size of 0.5 μm or 50 μm × 50 μm with a step size of 0.05 μm. The average sizes of grains and particles from TEM micrographs were measured by an NIS-Elements 3.1 software.

3 Results

3.1 Vickers microhardness

The evolution of Vickers microhardness during isochronal annealing after ECAP is shown in Fig. 2. The deformation induced by ECAP results in a significant increase of microhardness in both materials [21]. A moderate increase of microhardness occurs in Material A below 150 ℃ and is followed by a two-stage drop. However, only two-stage decrease of microhardness without any observable increase can be recognized in Material B. The first stage of microhardness drop is more pronounced in the as-cast Material A.

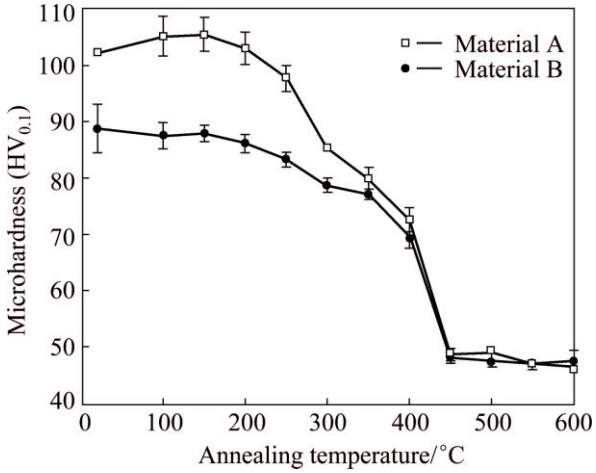

Fig. 2 Evolution of Vickers microhardness during isochronal annealing with heating scheme of 50 K/50 min

The values of microhardness are comparable for both materials at 400 ℃; final drop is observed at 450 ℃. Above this temperature, the values of microhardness are similar for both specimens within the limits of the experimental error and remain constant during further annealing.

3.2 EBSD measurement

EBSD measurements reveal elongated grain structure in both as-cast Material A and Material B annealed at 450 ℃. The length of grains in the casting direction is in the order of hundreds of micrometers and their thickness in normal direction is ~50 μm (Fig. 3(a)). ECAP processing results in a substantial grain refinement in both materials. The subgrain size decreases to approximately 0.5 μm (Fig. 3(b)). The ultra-fine grained structure remains stable up to 400 ℃ with no change of the grain size (Fig. 3(c)). Further isochronal annealing at 450 ℃ leads to the creation of a bimodal grain structure with larger grains with a diameter of ~50 μm and smaller ones with the average diameter of 10 μm (Fig. 3(d)). The average grain sizes measured by EBSD are comparable in both materials, thus, only microstructures from Material B are represented in Fig. 3.

3.3 TEM observation

TEM observations show that both materials contain a large number of subgrains with the average size lower than 500 nm after 4 ECAP passes (Figs. 4(a) and 5(a)). The dislocation density is much higher in Material A than in Material B.

Another significant difference between Materials A and B is the presence of secondary particles of Al_3Zr and α-Al(Mn,Fe)Si phases, which formed during pre-annealing at 450 ℃ and can be observed only in Material B. Some of the α-Al(Mn,Fe)Si particles are marked in Fig. 5(a).

The dislocation substructure inside grains of Material A is nearly fully recovered during annealing at temperatures not higher than 200 ℃ (Figs. 4(b) and (c)). New particles of α-Al(Mn,Fe)Si phase nucleate at above 250 ℃ in this material, preferentially on subgrain boundaries. Their average diameter increases to ~100 nm due to the further annealing (Fig. 6). At 400 ℃, their volume fraction reaches the maximum, later on dissolution of particles back to the solid solution prevails. As their average diameter remains constant, their volume fraction decreases. At 500 ℃ only small numbers of coarser particles remain undissolved (Fig. 4(f)).

The average size of precipitates in Material B slightly increases at above 350 ℃ (Fig. 6). No new particles precipitate during the in-situ annealing at higher temperatures, only coarsening and dissolution of existing ones occur (Fig. 5).

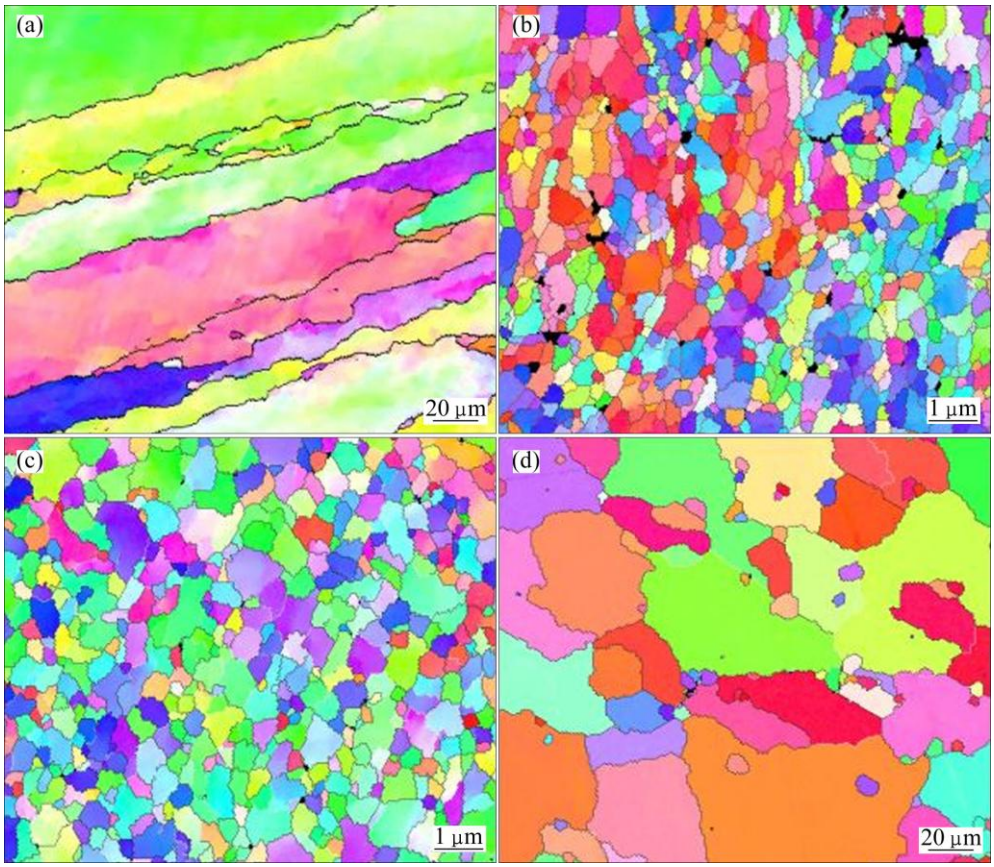

Fig. 3 EBSD maps of Material B in initial state (a), after 4 ECAP passes (b) and after annealing up to 400 ℃ (c) and 450 ℃ (d)

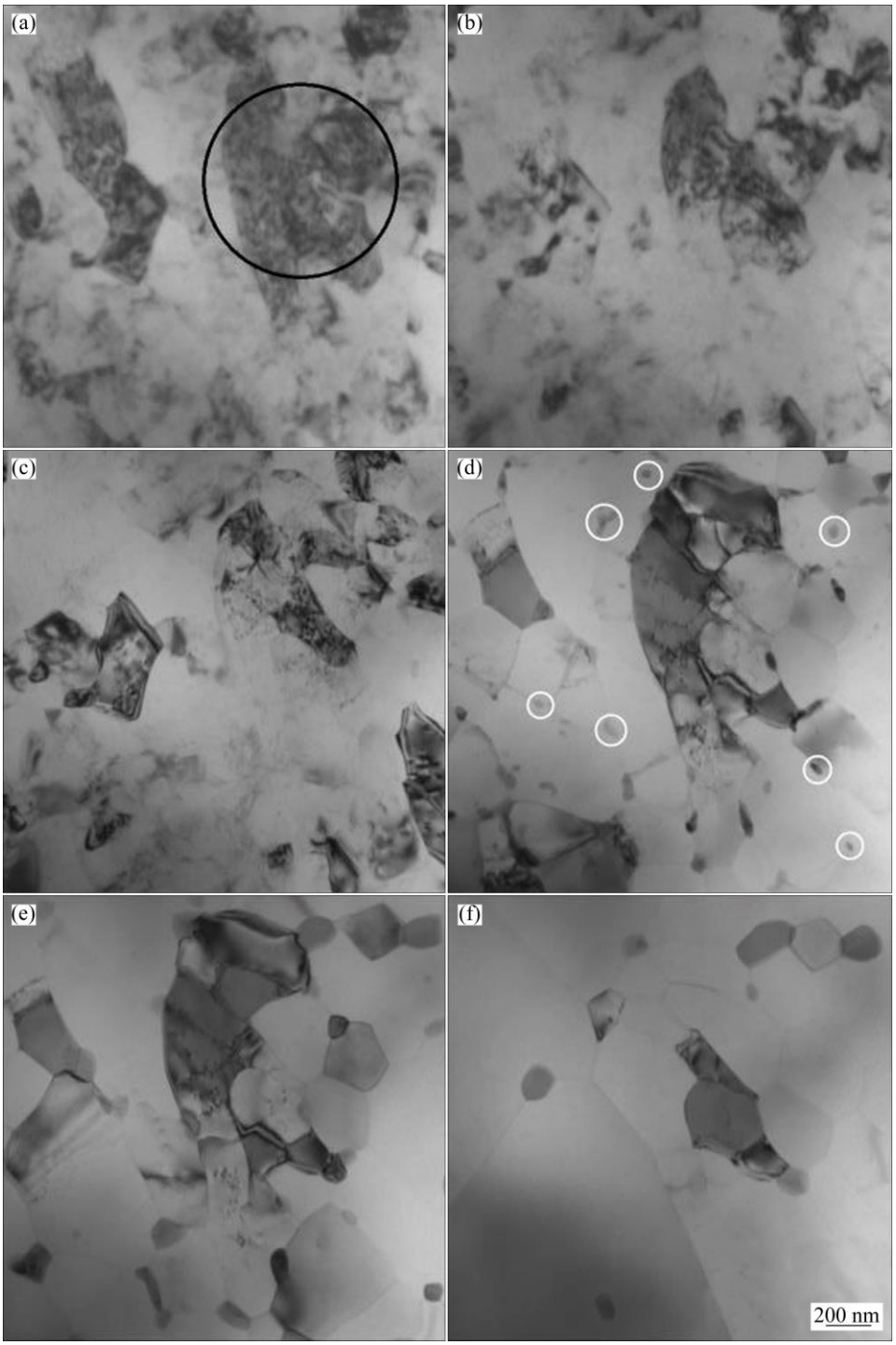

Fig. 4 TEM images of Material A after 4 ECAP passes (a) and during in-situ annealing up to 150 ℃ (b), 200 ℃ (c), 300 ℃ (d), 400 ℃ (e) and 500 ℃ (f) (Some α-Al(Mn,Fe)Si precipitates formed during annealing are marked by circles in (d))

The evolution of grain size is similar in both materials during in-situ annealing (Fig. 7). Up to 400 ℃ the subgrain size remains stable. At annealing temperature around 450 ℃, the significant subgrain growth occurs, forming a bimodal structure, i.e., a small amount of grains retain its sub-micron size while most of the matrix is composed of large grains with the average size of several microns.

4 Discussion

Annealing at 450 ℃ is responsible for microstructure differences between both studied materials. The microhardness of Material A is higher after ECAP than that observed in Material B. This is due to a higher work hardening rate and a limited dynamic

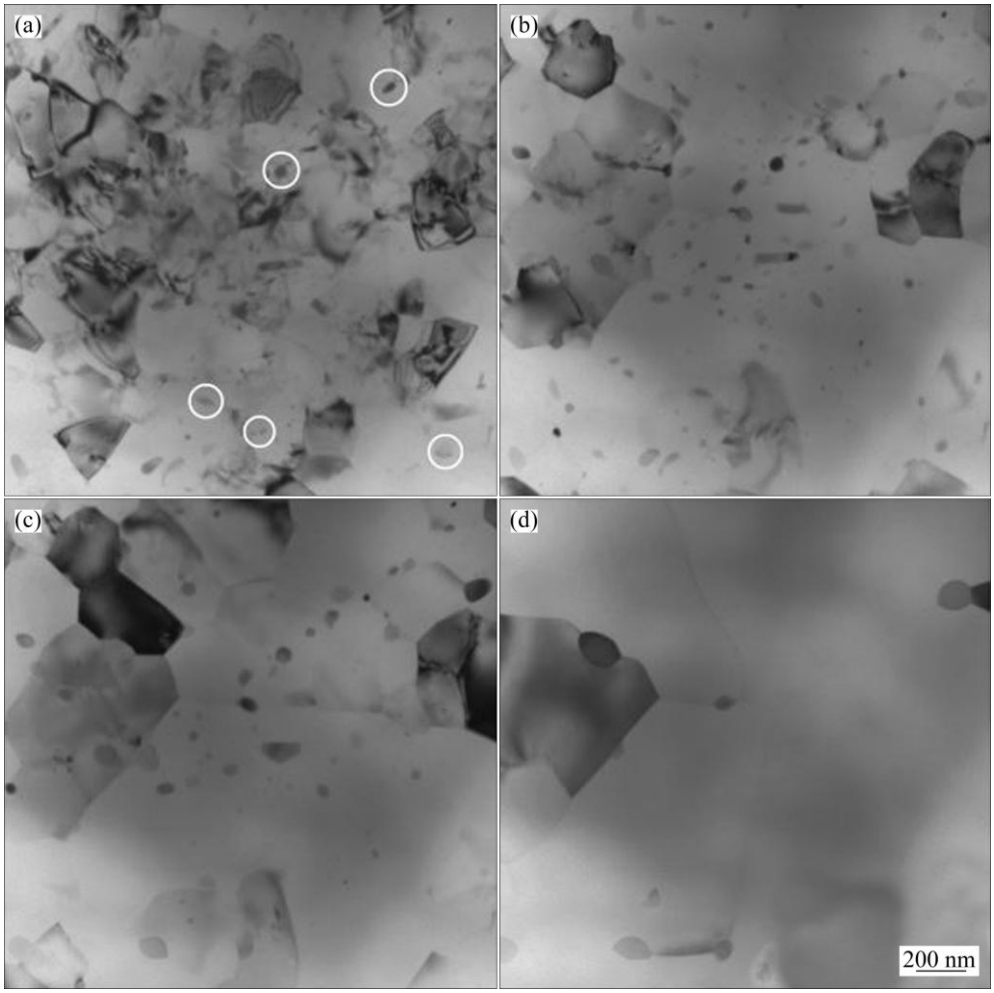

Fig. 5 TEM images of Material B after 4 ECAP passes (a) and during in-situ annealing at 300 ℃ (b), 400 ℃ (c) and 500 ℃ (d) (Circles in (a) indicate some α-Al(Mn,Fe)Si precipitates formed during pre-ECAP annealing at 450 ℃)

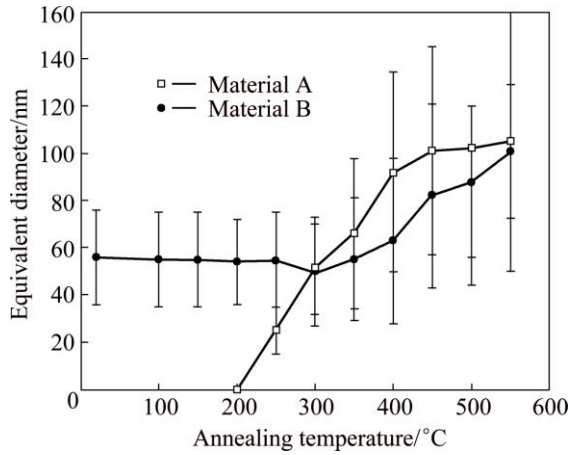

Fig. 6 Evolution of equivalent diameter of α-Al(Mn,Fe)Si particles measured during in-situ annealing

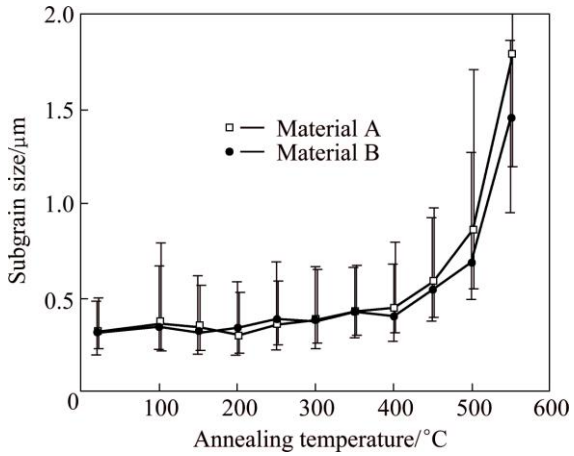

Fig. 7 Evolution of average subgrain size measured during in-situ annealing

recovery caused by a large amount of manganese dissolved in the aluminum matrix.

The initial deformed microstructure after ECAP processing has an influence on hardening and softening at elevated temperatures. The initial faint increase of microhardness observed in Material A below 150 ℃ might be associated with the mechanism described by HUANG et al [22] in a heavily deformed aluminum and observed also in other aluminum alloys [23]. The decrease of the dislocation density in such materials can

result in the surprising raise of the strengths in the initial stages of the dislocation recovery. As the dislocation density is decreased, new dislocation sources need to be activated to enable deformation and, thus, the strength of the material increases. Nevertheless, above 200 ℃ a formation of well defined subgrains occurs and microhardness finally decreases. No such increase of microhardness was observed in Material B, because it contained small subgrains with well developed subgrain boundaries.

The microhardness of Material B is lower after ECAP than that of Material A. The amount of dissolved atoms in aluminum matrix is lower and dynamic recovery during ECAP could proceed to higher extent in Material B than in Material A, as the dissolved Mn atoms serve as obstacles for the dislocation movement in Material A. Due to dynamic recovery, dislocation density after deformation is lower and the subgrains are better developed in the pre-annealed Material B and the extent of recovery in the course of post-ECAP annealing and connected microhardness drop are less significant than those of Material A.

The pronounced drop of microhardness between 400 ℃ and 450 ℃ is connected with the nucleation of new grains and full recrystallization. Both materials recrystallize at the same annealing temperature. Even isothermal annealing does not reveal any differences in the recrystallization kinetics between as-cast and pre-annealed alloys [24]. Because the presence of Al_3Zr particles generally shifts the recrystallization of deformed aluminum materials to higher temperatures by approximately 100 ℃ [25], different mechanisms have to be assigned to the improved recrystallization resistance of Material A. HUANG et al [26] have shown that recrystallization in cold-rolled aluminum alloys could be suppressed if the level of manganese in solid solution is high and a concurrent precipitation of Mn-rich particles creates effective obstacles for the grain boundary motion. Thus, the precipitation of α-Al(Mn,Fe)Si phase can, in accordance with previous observations [27], postpone recrystallization to higher temperatures (by approximately 100 ℃) in comparison with materials where the second phase particles are present already before deformation.

Moreover, even if no Al_3Zr precipitates were observed in Material A at 450 ℃ by TEM, their presence in the form of very small particles (diameter less than 1 nm) could not be excluded. Their eventual presence is very probable because annealing temperature and time are similar to the initial conditions of the Al_3Zr particle formation in Material B. Therefore, their role as recrystallization inhibitors could not be omitted.

According to in-situ TEM observations, recrystallization is also influenced by the dissolution of secondary particles. Because precipitates form mainly on subgrain boundaries, the motion of boundaries is hindered by these particles. Nevertheless, precipitates in both materials have already dissolved at 450 ℃ or they are too coarse to effectively pin grain boundaries and recrystallization can easily proceed.

5 Conclusions

1) The in-situ TEM observations were used for direct investigation of the precipitation processes and recrystallization of a modified twin-roll cast AA3003 aluminum alloy after ECAP.

2) In the annealed material, the recrystallization is retarded by Al_3Zr precipitates formed during the pre-annealing.

3) In the non-annealed material the recrystallization is postponed by a co-precipitation of α-Al(Mn,Fe)Si particles.

4) The higher value of microhardness in the non-annealed material is caused by higher work hardening rate during ECAP induced by solid solution saturation and consequently higher residual dislocation density in the subgrain interior.

5) The microhardness decrease during annealing in the non-annealed material is caused by both recovery and recrystallization, while that in the annealed material is caused preferentially only by recrystallization.

Acknowledgement

The financial supports of grants GAČR P107-12-0921 and SVV-2015-260213 are gratefully acknowledged.

References

[1] HORITA Z, FUJINAMI T, NEMOTO M, LANGDON T G. Improvement of mechanical properties for al alloys using equal-channel angular pressing [J]. Journal of Materials Processing Technology, 2001, 117: 288−292.

[2] NIKULIN I, KIPELOVA A, MALOPHEYEV S, KAIBYSHEV R. Effect of second phase particles on grain refinement during equal-channel angular pressing of an Al−Mg−Mn alloy [J]. Acta Materialia, 2012, 60: 487−497.

[3] NING J L, JIANG D M, FAN X G, LAI Z H, MENG Q C, WANG D L. Mechanical properties and microstructure of Al−Mg−Mn−Zr alloy processed by equal channel angular pressing at elevated temperature [J]. Materials Characterization, 2008, 59: 306−311.

[4] IWAHASHI Y, HORITA Z, NEMOTO M, LANGDON T G. An investigation of microstructural evolution during equal-channel angular pressing [J]. Acta Materialia, 1997, 45: 4733−4741.

[5] CABIBBO M. Microstructure strengthening mechanisms in different equal channel angular pressed aluminum alloys [J]. Materials Science and Engineering A, 2013, 560: 413−432.

[6] CIESLAR M, SLÁMOVÁ M, UHLÍŘ J, COUPEAU C, BONNEVILLE J. Effect of composition and work hardening on solid solution decomposition in twin-roll cast Al−Mn sheets [J]. Kovové

Materiály (Metallic Materials), 2007, 45: 91−98.
[7] LIU W, RADHAKRISHNAN B. Recrystallization behavior of a supersaturated Al−Mn alloy [J]. Materials Letters, 2010, 64: 1829−1832.
[8] POKOVÁ M, CIESLAR M, LACAZE J. The influence of silicon content on recrystallization of twin-roll cast aluminum alloys for heat exchangers [J]. Acta Physica Polonica A, 2012, 122: 625−629.
[9] BIROL Y. Response to annealing treatment of a twin-roll cast thin AlFeMnSi strip [J]. Journal of Materials Processing Technology, 2009, 209: 506−510.
[10] GRAS C, MEREDITH M, HUNT J D. Microstructure and texture evolution after twin roll casting and subsequent cold rolling of Al−Mg−Mn aluminium alloys [J]. Journal of Materials Processing Technology, 2005, 169: 156−163.
[11] SLÁMOVÁ M, KARLÍK M, CIESLAR M, CHALUPA B, MERLE P. Structure transformation during annealing of twin-roll cast Al−Fe−Mn−Si (AA8006) alloy. Sheets I: Effect of cold rolling and heating rate [J]. Kovové Materiály (Metallic Materials), 2002, 40: 389−400.
[12] KANG H G, LEE J P, HUH M Y, ENGLER O. Stability against coarsening in ultra-fine grained aluminum alloy AA3103 sheet fabricated by continuous confined strip sheering [J]. Materials Science and Engineering A, 2008, 486: 470−480.
[13] VLACH M, ČÍŽEK J, MELIKHOVÁ O, STULÍKOVÁ I, SMOLA B, KEKULE T, KUDRNOVÁ H, GEMMA R, NEUBERT V. Early stages of precipitation process in Al−(Mn−)Sc−Zr alloy characterized by positron annihilation [J]. Metallurgical and Materials Transaction A, 2015, 46: 1156−1564.
[14] CLOUET E, LA L, EPICIER T, LEFEBVRE W, NASTAR M, DESCHAMPS A. Complex precipitation pathways in multicomponent alloys [J]. Nature Materials, 2006, 5: 482−488.
[15] KARLÍK M, MÁNIK T, LAUSCHMAN H. Influence of Si and Fe on the distribution of intermetallic compounds in twin-roll cast Al−Mn−Zr alloys [J]. Journal of Alloys and Compounds, 2012, 515: 108−113.
[16] KARLÍK M, MÁNIK T, SLÁMOVÁ M, LAUCHMANN H. Effect of Si and Fe on the recrystallization response of Al−Mn alloys with Zr addition [J]. Acta Physica Polonica A, 2012, 122: 469−474.
[17] POKOVÁ M, CIESLAR M, LACAZE J. TEM investigation of precipitation in Al−Mn alloys with addition of Zr [J]. Manufacturing Technology, 2012, 12: 212−217.
[18] POKOVÁ M, ZIMINA M, CIESLAR M. Microstructure evolution of AA3003 aluminum alloys enhanced by zirconium addition studied by electron microscopy [J]. Light Metals, 2015, 2015: 469−474.
[19] MUGGERUD A M F, LI Y, HOLMESTAD R. Orientation studies of α-Al(Fe,Mn)Si dispersoids in 3xxx Al alloys [J]. Materials Science Forum, 2014, 794−796: 39−44.
[20] GAO T, WU Y, LI C, LIU X. Morphologies and growth mechanisms of α-Al(FeMn)Si in Al−Si−Fe−Mn alloy [J]. Materials Letters, 2013, 110: 191−194.
[21] MÁLEK P, POKOVÁ M, CIESLAR M. The influence of ECAP on mechanical properties of a twin-roll cast Al−Mn−Fe−Si−Zr alloy [C]//Proceedings of Metal 2014 Conference. Brno, 2014: 247−252.
[22] HUANG X, KAMIKAWA N, HASEN N. Strengthening mechanism in nanostructured aluminium [J]. Materials Science and Engineering A, 2008, 483−484: 102−104.
[23] CIESLAR M, POKOVÁ M. Annealing effects in twin-roll cast AA8006 aluminium sheets processed by accumulative roll-bonding [J]. Materials, 2014, 7: 8058−8069.
[24] POKOVÁ M, ZIMINA M, CIESLAR M. The evolution of microstructure and mechanical properties of Al−Mn−Fe−Si alloys during isothermal annealing [J]. Acta Physica Polonica A, 2015, 128: 746−749.
[25] POKOVÁ M, CIESLAR M. Study of twin-roll cast aluminium alloys subjected to severe plastic deformation by equal channel angular pressing [J]. Materials Science and Engineering: IOP Conference Series, 2014, 62: 012086.
[26] HUANG K, LI Y J, MARTHINSEN K. Effect of heterogeneously distributed pre-existing dispersoids on the recrystallization behavior of a cold-rolled AlMnFeSi alloy [J]. Materials Characterization, 2015, 102: 92−97.
[27] POKOVÁ M, CIESLAR M, SLÁMOVÁ M. The influence of dispersoids on the recrystallization of aluminium alloys [J]. International Journal of Materials Research, 2009, 100: 391−394.

预退火处理对等通道转角挤压双辊铸轧 AA3003 铝合金显微组织演变的影响

Michaela Šlapáková POKOVÁ, Mariia ZIMINA, Miroslav CIESLAR

Faculty of Mathematics and Physics, Charles University in Prague, Ke Karlovu 5, 121 16 Prague 2, Czech Republic

摘　要：添加少量锆元素对双辊铸轧 AA3003 铝合金进行改性。在 450 ℃ 对合金进行退火处理产生 Al_3Zr 析出相，同时出现富 Mn α-Al(Mn, Fe)Si 相。由等通道转角挤压引起的大塑性变形致使合金的晶粒细化且硬度增加。电子背散射衍射及透射电镜观察结果显示在热处理变形后期预先退火处理对合金显微组织变化的影响。对于变形前未进行退火处理的合金，在 450 ℃ 退火时，其位错回复和 α-Al(Mn, Fe)Si 相析出使再结晶提前发生。由于预变形退火使固溶体中 Mn 原子含量降低，因此，在变形过程中对合金进行预变形退火处理会使回复更容易发生。Al_3Zr 析出相能促进再结晶过程的进行。

关键词：铝合金；Al_3Zr；α-Al(Mn, Fe)Si；预退火；回复；再结晶；组织演变

(Edited by Wei-ping CHEN)